JACS
JOURNAL OF THE AMERICAN CHEMICAL SOCIETY
Article
pubs.acs.org/JACS

Hexane-Driven Icosahedral to Cuboctahedral Structure Transformation of Gold Nanoclusters

Yuanyuan Li,[†] Hao Cheng,[†] Tao Yao,[†] Zhihu Sun,*[,†] Wensheng Yan,[†] Yong Jiang,[†] Yi Xie,*[,‡] Yongfu Sun,[‡] Yuanyuan Huang,[†] Shoujie Liu,[†] Jing Zhang,[§] Yaning Xie,[§] Tiandou Hu,[§] Lina Yang,[†] Ziyu Wu,[†] and Shiqiang Wei*[,†]

[†]National Synchrotron Radiation Laboratory, University of Science and Technology of China, Hefei, Anhui 230029, P.R. China

[‡]Department of Nanomaterials and Nanochemistry, Hefei National Laboratory for Physical Sciences at Microscale, University of Science and Technology of China, Hefei 230026, P.R. China

[§]Beijing Synchrotron Radiation Facility, Institute of High Energy Physics, Chinese Academy of Sciences, Beijing 100049, P.R. China

Supporting Information

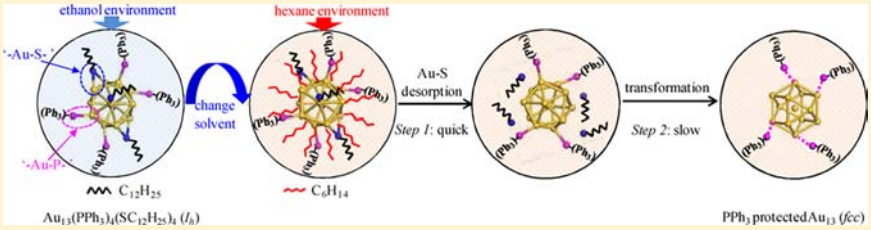

ABSTRACT: Whether and how nanoclusters possessing a rich diversity of possible geometric configurations can transform from one structural type to another are critical issues in cluster science. Here we demonstrate an icosahedral-to-cuboctahedral structural transformation of Au nanoclusters driven by changing the chemical environment. For icosahedral Au_{13} clusters protected by a mixture of dodecanethiol and triphenylphosphine ligands, solvent exchange of ethanol by hexane leads to quick selective desorption of the thiolate layers from the cluster surface. The surviving Au cores then undergo a much slower energy-minimization process via structural rearrangement, stabilized in the cuboctahedral structure and protected by triphenylphosphine in the hexane environment. In response to the dramatically changed atomic structure, the character of the electronic structure of the Au clusters is converted from semiconducting to metallic. This work addresses the structure–property correlation and its strong dependence on the chemical environment for metal nanoclusters.

INTRODUCTION

Metal nanoclusters acting like "superatoms" exhibit fascinating physicochemical properties with promising applications in a variety of areas such as photonics, catalysis, sensing, and medicine.[1−7] Among them, Au nanoclusters stabilized by organic molecules such as phosphine (PR_3) and thiolate (SR) ligands have been regarded as a model system. Following the so-called "phosphine chemistry" period in which Au nanoparticles with core sizes in the 1−3 nm range were stabilized by phosphines, tremendous efforts have been made in synthesizing Au nanoparticles stabilized by thiolates. The first chemical preparation of 2−5-nm SR-protected Au clusters by Brust et al.[8] spurred the rapid development of "thiolate chemistry".[9−13] Recent breakthroughs in the total structure determination for the SR- or PR_3-capped Au_{25},[14,15] Au_{38},[16] and Au_{102}[13] clusters have revealed the uniqueness of the Au cluster structures: the thiolates do not merely coat the uppermost Au layer but rather form Au–thiolate oligomers anchored on the Au cores. As a result, the Au cores of the clusters adopt molecule-like atomic structures that are completely different from the face-centered cubic (*fcc*) packing of bulk Au. Taking the Au_{38} cluster as an example, a diverse set of structures has been experimentally observed or theoretically predicted. These include disordered[17−19] symmetric configurations with cores in different symmetry (such as bi-icosahedral Au_{23},[16,20] O_h Au_{14}[21]), or a truncated octahedral *fcc* Au_{38} geometry.[22,23] These unique atomic structures determine the intriguing electronic structures and other physical and chemical properties of the clusters.[24] Then whether the clusters can transform from one structural type to another and how to achieve this transformation are critical issues in cluster science.[25] The structural tunability also provides a means to manipulate the properties of the clusters, a subject of great importance in the advancement of nanotechnology.

The atomic structures of ligand-protected Au clusters are tightly correlated with the interactions between the core and surface Au atoms; thus, manipulating the structure and property of Au clusters might be realized by alternating the surface Au–ligand bonds. Generally, this relies strongly on the full understanding and controllable modifications of the surface chemistry, mainly in terms of the ligands and solvents.[26]

Received: July 16, 2012
Published: October 10, 2012

   dx.doi.org/10.1021/ja306923a | J. Am. Chem. Soc. 2012, 134, 17997−18003

However, previous studies show that the core structure of $Au_{25}(SCH_2CH_2Ph)_{18}$ clusters remain intact upon ligand–exchange of SCH_2CH_2Ph– with *p*-substituted arylthiols (*p*-X-PhSH, where X = NO_2, Br, CH_3, OCH_3, and OH).[27] Instead, it was found that the stability and surface activity of hexanethiolate-protected Au_{38} cluster are critically dependent on the solvent, but the solvent-induced structural changes are not clarified.[28] MacDonald et al. studied the solvation effects of thiolate-protected Au_{38} clusters,[29,30] and reported a significant bond expansion in the solution-phase clusters. For other nanosystems, it is also starting to emerge that their atomic-scale structure and properties are intimately tied to the nature of the environment.[31] For example, the organization of gold nanorods could be tuned by solvent in a controllable way[32,33] and 3-nm ZnS nanocrystals experience a structural transition after binding to water at room temperature.[34] All these findings highlight the importance of solvent in tuning the structure and properties of nanomaterials, which is especially essential for ultrasmall Au clusters due to their strong reliance on the surface chemistry.

In this work, we demonstrate for the first time that the structural transition of gold nanoclusters could be achieved by a solvent-exchange method. Mixed thiolate/phosphine-protected Au_{13} nanoclusters are found to undergo an icosahedral-to-cuboctahedral structure transformation as revealed by in-depth analysis of X-ray and UV–vis absorption spectra. The underlying reason for the dramatic change of atomic structure is also clarified. Accompanied with the atomic structure changes, the character of the electronic structure transits from semiconducting to metal-like, indicating a strong structure–property relationship. This work also sheds light on the understanding of structural transitions during the evolution of clusters to nanocrystals, a fundamental scientific problem that remains to be elucidated.[35]

EXPERIMENTAL SECTION

Samples. Au nanoclusters with high monodispersity were prepared following a "precursor self-supply" method.[36] The synthesis details involve the reduction of the precursor $AuClPPh_3$ (0.375 mmol) by *tert*-butylamine-borane (3.75 mmol) in the ethanol (21 mL) solvent at room temperature under vigorous stirring. At 60 min after the addition of a reducing agent, the surfactant (48 μL of dodecanethiol) was injected to protect the clusters. The effects of the solvent-exchange process on the Au clusters were examined by subsequent measurements.

In Situ X-ray Absorption Fine Structure (XAFS) Measurements. The Au L_3-edge XAFS spectra were measured at the U7C beamline of the National Synchrotron Radiation Laboratory (NSRL), China, and the 1W1B beamline of Beijing Synchrotron Radiation Facility (BSRF), China. The storage ring of NSRL was working at the energy of 0.8 GeV and a maximum electron current of 300 mA, and the storage ring of BSRF was operating at 2.5 GeV with a maximum current of 250 mA. XANES measurements were conducted in transmission and quick-scan mode (1 min per scan) in the energy range from 50 below to 100 eV above the Au L_3-edge. After the clusters were dispersed in hexane, the solution was quickly taken from the flask at different times and then transferred to a 10-mm-thick Teflon cell for the XANES measurements.

Transmission Electron Microscopy and in Situ UV–Vis Measurements. TEM and in situ UV–vis were performed at the University of Science and Technology of China. TEM images were obtained with a JEM-2100F system. The samples for TEM were prepared by dropping the reaction solution onto copper TEM grids directly and drying in air. The in situ UV–vis absorption spectra were recorded with a Shimadzu SOLID3700 spectrophotometer in the wavelength range of 300–800 nm and corrected by pure ethanol or hexane as background absorption. As a reference, the initial precursor solution was also measured.

Matrix-Assisted Laser Desorption Ionization Time-of-Flight Mass-Spectrometry (MALDI-TOF MS) Measurements. Mass spectra were measured with a Bruker Autoflex III mass spectrometer in positive linear mode. The Au cluster samples were mixed with matrix *trans*-2-[3-(4-*tert*-butylphenyl)-2-methyl-2-propenyldidene]-malononitrile (DCTB) in the ratio of 1:1000. Then one or two microliters of the mixture was applied to the sample plate and air-dried. In our measurements, the range of m/z was tuned from 0 to 20000.

RESULTS AND DISCUSSION

Hexane-Induced Structure Change of Au Nanoclusters. To demonstrate the impact of changed chemical environment on the Au clusters, we display in Figure 1a the

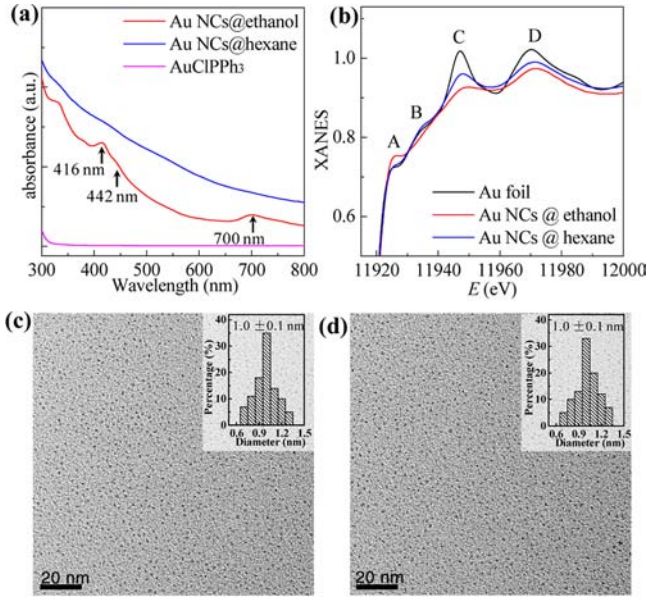

Figure 1. Unexpected spectral variation for Au clusters in ethanol and hexane. (a) UV–vis absorption spectra of the precursor, Au nanoclusters in ethanol and in hexane. (b) XANES of Au foil, Au nanoclusters in ethanol and in hexane. TEM images of Au nanoclusters (c) in ethanol and (d) in hexane.

UV–vis absorption spectra for the clusters in different solvents of ethanol and hexane. For the as-prepared clusters in ethanol, the spectral profile is highly structured, with steplike multiple absorption bands peaked at the wavelengths of 416, 442, and 700 nm. These multiple absorption bands, totally different from the characteristic surface plasmon resonance (SPR) absorbance (at ~520 nm) for Au nanocrystals, are the fingerprint features of Au clusters with molecule-like electronic structure. The 700-nm absorption peak indicates the energy gap of 1.8 eV between the highest occupied molecular orbital (HOMO) and the lowest unoccupied molecular orbital (LUMO), indicating the semiconducting character that is commonly observed for ligand-protected Au clusters.[15,16,37,38] However, upon dispersing the Au clusters in hexane, all these characteristic peaks are smeared out, and the absorption profile becomes almost featureless. It has been known that in some cases the optical absorption features of nanoparticles might be modified by the change in the dielectric of the environment with different refractive indices,[39] but numerous experimental results revealed that pure solvent effects could only lead to shifts in the

dx.doi.org/10.1021/ja306923a | J. Am. Chem. Soc. 2012, 134, 17997–18003

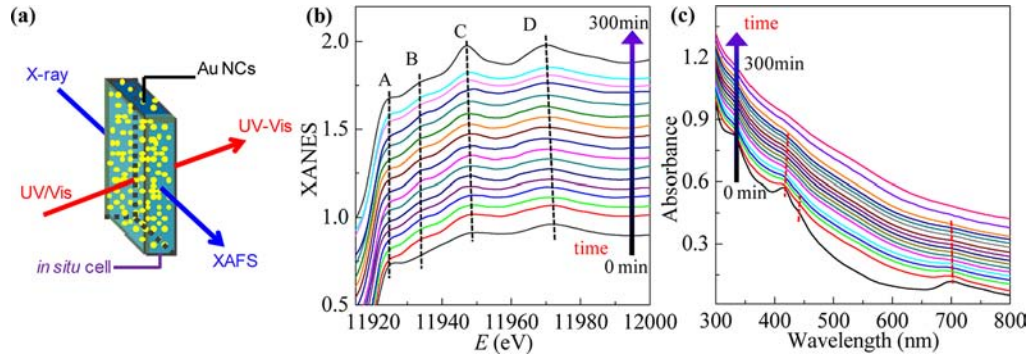

Figure 2. Process of structural transformation. (a) Schematic presentation of the experimental setup employed for in situ XANES and UV−vis measurements of Au nanoclusters. Time-dependent (b) XANES and (c) UV−vis absorption spectra for Au nanoclusters redispersed in hexane.

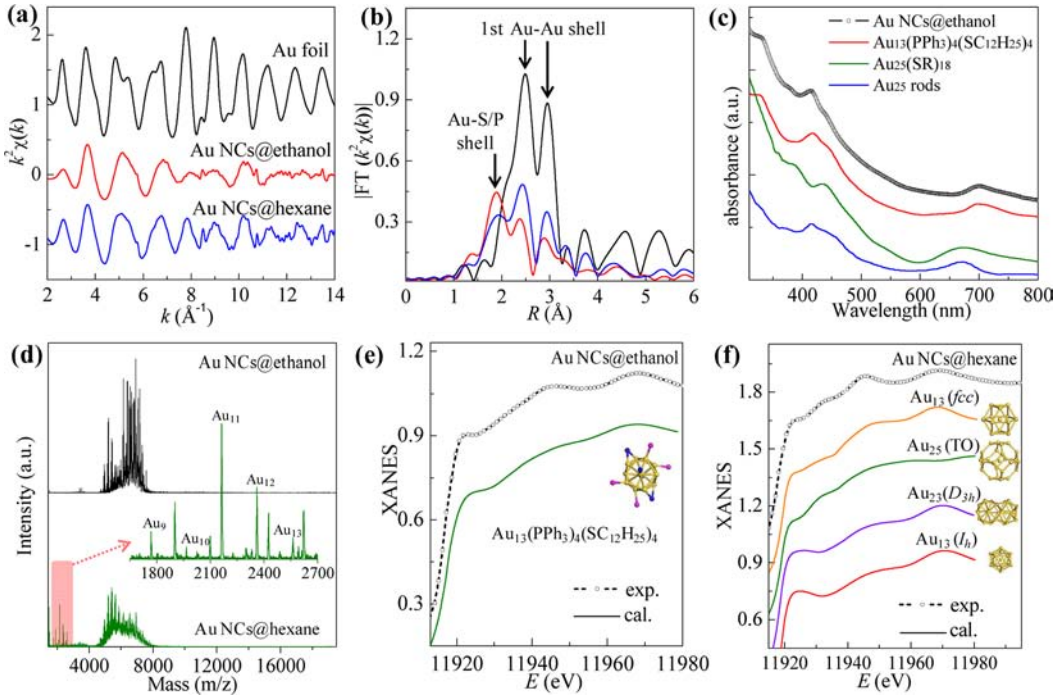

Figure 3. Structure determination of Au nanoclusters. (a) EXAFS $k^2\chi(k)$ and (b) Fourier-transformed $k^2\chi(k)$ functions of Au foil, Au nanoclusters in ethanol and in hexane. (c) The UV−vis spectra of Au clusters in ethanol, standard icosahedral $Au_{13}(PPh_3)_4(SC_{12}H_{25})_4$ (from ref 50), bi-icosahedral $Au_{25}(SR)_{18}$ (from ref 51), and Au_{25} nanorod clusters (from ref 52). (d) The MALDI-TOF MS spectra of Au nanoclusters in ethanol and hexane. (e) The structure of $Au_{13}(PPh_3)_4(SC_{12}H_{25})_4$ cluster with an I_h core and comparison of its calculated XANES spectrum with that of Au clusters in ethanol. (f) The structure of SR-free Au clusters with different geometric symmetry of the Au core: I_h Au_{13} cluster, D_{3h} Au_{23} cluster, truncated octahedral Au_{25} cluster, and *fcc* Au_{13} cluster, and comparison of their corresponding calculated XANES spectra with those of Au clusters in hexane.

absorption peak position while the spectral shapes are kept unchanged.[40,41] The very recent density functional theory calculations on thiolate-protected Au_{25} nanoclusters by Aikens have also demonstrated that solvent has negligible effects on the features of optical absorption, and the core geometric and electronic structure is the primary determinant for the discrete optical absorption.[42] Hence, it is most possible that the changed optical absorption features are attributed to hexane-induced electronic/atomic structure changes.

Insights into the hexane-induced changes of the Au nanoclusters could be obtained by means of X-ray absorption fine structure (XAFS, including XANES and EXAFS).[29,30,43,44] We first show the Au L_3-edge XANES spectra in Figure 1b. As compared with the *fcc*-structured Au foil, the clusters in ethanol exhibit much more intense white-line peak (corresponding to the electronic transition from the $2p_{3/2}$ to the $5d_{5/2,\ 3/2}$ states) at around 11926 eV, while all the other peaks are shifted in energy and reduced in intensity. The peak at 11934 eV that is apparent for Au foil is absent for the clusters. The significantly different XANES feature relative to Au foil indicates that the atomic packing of the Au clusters is far from the *fcc* structure, in line with the molecule-like structure of clusters as revealed by UV−vis spectra. However, after hexane dispersal, the spectral shape undergoes a great change and becomes very similar to that of Au foil, except for some reduction in the peak intensities and slight shifts in energy. This indicates the basic *fcc* atomic packing of the clusters upon hexane dispersal, thanks to the "phase fingerprint" ability of XANES in distinguishing specific structural information.

In order to determine if the sizes of the clusters have been changed severely by the solvent exchange, we measured the TEM images as shown in Figure 1c,d. One can see that neither

dx.doi.org/10.1021/ja306923a | J. Am. Chem. Soc. 2012, 134, 17997−18003

Table 1. Structural Parameters Extracted from Quantitative EXAFS Curve-Fitting

sample	bond	R (Å)	N	σ^2 (10^{-3} Å)	ΔE (eV)
Au-foil	Au−Au	2.88 ± 0.01	12	8.1 ± 0.4	2.4 ± 0.4
Au clusters@ethanol	Au−S/P	2.31 ± 0.03	0.9 ± 0.2	3.2 ± 0.3	3.2 ± 0.3
	Au−Au	2.82 ± 0.02	6.5 ± 0.3	10.2 ± 0.7	2.2 ± 0.2
Au clusters@hexane	Au−P	2.33 ± 0.02	0.4 ± 0.2	3.5 ± 0.2	3.8 ± 0.4
	Au−Au	2.83 ± 0.03	6.5 ± 0.8	8.2 ± 0.5	2.7 ± 0.3

the mean size (1.0 nm) nor the size distribution (0.1 nm) is noticeably changed by the solvent exchange. This is not surprising since hexane has long been widely used as an organic medium to disperse metal nanoparticles and is believed not to alter their sizes. Hence, the great changes in the UV−vis and X-ray absorption spectra of the clusters upon dispersal in hexane are not due to the size effect but result from some inherent structural transformations of the clusters. Accordingly, we conclude that the solvent-induced changes of the UV−vis and X-ray absorption spectra are primarily due to the rearrangement of the atomic structures of the clusters from molecule-like configuration to *fcc* packing, which renders different electronic structures as a natural result.

Time-Dependent Process of the Structural Transformation. To monitor the changes of electronic and geometric structures of Au clusters after dispersing in hexane, time-dependent Au L_3-edge XANES and UV−vis absorption spectra were measured (Figure 2a). We first discuss the XANES spectra (Figure 2b) which exhibit four characteristic peaks A−D bearing close relation to the electronic structure and geometric configuration of the clusters. After 3 min of dispersal in hexane, peak A is greatly reduced, peak B becomes more pronounced, and the spectrum resembles that of *fcc*-structured Au bulk. This demonstrates that dispersal in hexane leads to a quick variation of electronic and atomic structures. After that, no changes in the overall spectral profile could be observed, except for slight shifts of peaks B, C, and D to get closer to those of Au foil. Similar temporal evolution is also revealed by time-dependent UV−vis absorption spectra (Figure 2c). Within 2 min of the clusters dispersing in hexane, the absorption peaks at around 416, 442, and 700 nm drop sharply in intensity. From 20 min on, the peak located at 442 nm disappears. Finally, the UV−vis absorption curve becomes almost featureless. Since these optical absorption peaks for ligand-protected Au clusters generally arise from the electron transition from occupied orbitals to unoccupied ones with a significant contribution of the ligand orbital,[15,42] their great change demonstrates the strong variation of electronic structure associated with the rearranged geometric configuration of the clusters.

The Driving Force for the Structural Transformation. The underlying reason of this hexane-induced geometric transformation could be further unraveled by EXAFS spectra (Figure 3a,b). The Fourier-transformed (FT) $k^2\chi(k)$ function for the Au clusters in ethanol demonstrates a strong Au−ligand peak located at 1.87 Å, together with relatively weaker Au−Au peaks in the range of 2.0−3.5 Å (Figure 3b). In the as-prepared Au clusters, the Au−ligand coordination may be Au−S and/or Au−P bonds that come from the protecting phosphines and thiolates or their mixture. Because S and P are neighboring elements in the Periodic Table of the elements and cannot be distinguished by EXAFS, for the sake of simplicity, we use Au−ligand coordination to represent all of them in the EXAFS analysis. Seen from Figure 3b, dispersing the as-prepared clusters in hexane leads to a remarkable amplitude reduction of the Au−ligand peak, while the Au−Au peaks are considerably increased in intensity. Quantitative least-squares curve-fitting (see the Supporting Information for the details) shows that the hexane treatment leads to a reduction of the averaged Au−ligand coordination number from 0.9 to 0.4 (Table 1), suggesting desorption of some of the ligands from the cluster surface.

It is most likely that dispersing the ligand-protected Au clusters in hexane has completely removed the thiolates from the cluster surface, while the phosphines remain to protect the Au cores. This claim is supported by two reasons. First, if some thiolates were still covering the *fcc* clusters, according to the theoretical calculations by Jiang et al.,[45] the clusters should exhibit semiconducting character, and hence, steplike optical absorption bands should appear, contrary to the experimental observation of the nearly featureless UV−vis absorption spectrum (Figure 1a). Experimental observations also indicated that the optical absorption spectra of fully phosphine-stabilized Au clusters are much less structured than thiolated Au clusters with the same size.[46] Second, the presence of S around Au clusters would also considerably increase the XANES white-line intensity due to the Au→S charge transfer,[47] and makes the XANES spectrum deviate from the *fcc* characteristics. On the contrary, for phosphine-stabilized Au clusters, the ligand has fewer effects on the white-line intensity[48] because of the weaker Au−P interactions relative to those of Au−S. According to the "divide and protect" concept,[13,21,49] a Au nanocluster, as a "superatom", is stable because the surface gold atoms in the core have at least one surface−chemical bond and the gold core exhibits a strong electron shell closing. Therefore, the removal of the protecting thiolates from the cluster surface makes the number of electrons deviate from the closing shell and destroys their stable electronic structures. Consequently, the original core structure of the clusters would destabilize, and a new *fcc* structure is adopted for minimization of the energy. In this case, the bulky phenyl groups of PPh_3 provided steric protections for the clusters.

Why hexane could remove the thiolate ligands from Au clusters is not fully understood now, but some clue could be found from its low solvent polarity (0.06) and solubility parameter (7.3). The strong hydrophobic interaction between hexane and the nonpolar hydrocarbon tail of dodecanethiol may be the driving force for desorption of thiolates from the metal core.

Atomic Structures of Au Nanoclusters before and after the Transformation. As we have mentioned, the UV−vis absorption spectrum of the as-prepared Au clusters in ethanol exhibits steplike absorption curves with characteristic multiple peaks at 416, 442, and 700 nm. It is worthy of note that highly structured optical absorption spectra are commonly observed for several different types of Au clusters (~1 nm), including bi-icosahedral $Au_{25}(SR)_{18}$ cluster,[15] $[Au_{25}(PPh_3)_{10}(SC_nH_{2n+1})_5Cl_2]^{2+}$ nanorod cluster,[52] icosahedral $Au_{13}(PPh_3)_4(SC_{12}H_{25})_2Cl_2$ and $Au_{13}(PPh_3)_4(SC_{12}H_{25})_4$ clus-

dx.doi.org/10.1021/ja306923a | J. Am. Chem. Soc. 2012, 134, 17997−18003

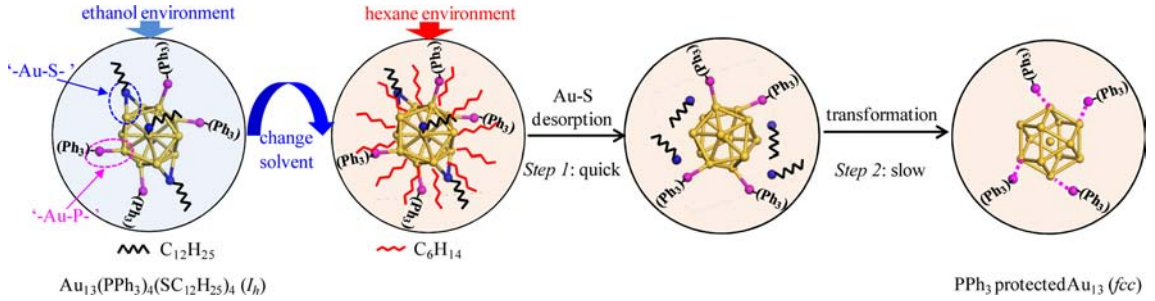

Figure 4. Schematic illustration of the two-step process of the structural transformation. The first step refers to the quick depletion of the ligands of the surface thiolates from the Au clusters upon hexane dispersal. In the second step, the PPh_3-stabilized Au clusters undergo a structural transformation to form *fcc*-structured clusters.

ters,[50] and fully thiolated Au_{11} cluster.[46] To show the differences, in the inset of Figure 3c we compare the UV−vis spectra of our clusters in ethanol with those of $Au_{13}(PPh_3)_4(SC_{12}H_{25})_4$, bi-icosahedral $Au_{25}(SR)_{18}$, and Au_{25} nanorod clusters. The spectra for $Au_{13}(PPh_3)_4(SC_{12}H_{25})_2Cl_2$ and fully thiolated Au_{11} clusters are identical to that of Au_{25} nanorod and are not shown. We can see that the $Au_{25}(SR)_{18}$ cluster has quite different absorption features than ours and could be excluded as a main component in our sample. Also, there is some noticeable difference between the spectra of our sample in ethanol and that of the Au_{25} nanorod cluster. The 700-nm absorption band (assigned to the HOMO−LUMO gap) of our clusters is significantly different from that (670 nm) for the Au_{25} nanorod. Such a 700-nm absorption band could only be found in the icosahedral $Au_{13}(PPh_3)_4(SC_{12}H_{25})_4$ cluster, which displays exactly the same spectral shapes and peak positions as our clusters do. We also used matrix-assisted laser desorption ionization time-of-flight mass-spectrometry (MALDI-TOF MS) to determine the molecular structure of the clusters (Figure 3d). Unfortunately, due to the presence of PPh_3 in our samples, the MALDI-TOF MS analysis shows a very wide mass peak centered at 6.5 kDa that mainly comes from ligand loss and fragmentation/recombination processes caused by the laser ionization of the clusters in the gas phase.[51] Instead, we resort to the XAFS analysis. Our experimental XANES spectrum, which is exactly the same as that reported by Menard et al.,[53] could be well reproduced on the basis of the atomic structure of the $Au_{13}(PPh_3)_4(SC_{12}H_{25})_4$ cluster (Figure 3e).[54] This is also consistent with the quantitative EXAFS results that the Au−S/P and Au−Au coordination numbers (0.9 and 6.5, Table 1) are very close to the values (0.76 and 6.7) in the $Au_{13}(PPh_3)_4(SC_{12}H_{25})_4$.[54,55] Since both UV−vis and XAFS spectra are regarded as spectroscopic fingerprints of Au clusters, our sample in ethanol could be identified as the icosahedral $Au_{13}(PPh_3)_4(SC_{12}H_{25})_4$ cluster.

As for the Au clusters in hexane, we have known that they adopt the *fcc* atomic packing after the structural transformation, but their precise atomic structure is still unclear. Some hints could be gained from XANES, due to its sensitivity to three-dimensional (3D) atomic structure. For this purpose, we calculated Au L_3-edge XANES spectra for several structural models of bare clusters. Au clusters (∼1 nm) with representative atomic packing (icosahedral,[14,15] bi-icosahedral,[16] truncated octahedral,[56] and *fcc*-like Au_{13}[57]) were considered, and the calculation results are displayed in Figure 3f. As expected, the spectral profiles are influenced greatly by the geometric structure of the Au core. The spectral shape of the clusters after the hexane treatment could not be reproduced by bare icosahedral Au clusters, such as Au_{13} or Au_{23}, and shows quite different features from that of truncated octahedral Au_{25} in the energy range of 11940−11980 eV (Figure 3f). Indeed, the simulated XANES spectrum for *fcc*-structured clusters such as cuboctahedral Au_{13} with the *fcc* atomic packing character could reproduce the main experimental features of the hexane-dispersed Au clusters. The MALDI-TOF MS analysis of the hexane-dispersed Au clusters also indicates the presence of small Au clusters consisting of 9−13 atoms (Figure 3d) in addition to the wide mass peak centered at 6.0 kDa. This provides support for the formation of Au_{13} clusters in hexane. The Au−Au coordination number (6.5) extracted from EXAFS analysis does not show a noticeable change, which means that, after hexane treatment, the cluster size does not increase significantly, in agreement with the TEM measurements. The DFT calculations also indicate that the cuboctahedral Au_{13} cluster exhibits a metallic behavior,[58] as inferred from the significant density of states (DOS) at the Fermi level. This is a natural result, considering the metallic behavior even for a Au_{13} core in a ligand-protected Au_n cluster.[30,59,60] In fact, the metallic behavior of the cuboctahedral Au_{13} cluster is in line with a common feature of 1−2-nm-sized *fcc* nanoparticles whose UV−vis absorption spectra show neither obvious SPR resonance for larger (>2 nm) nanocrystals nor molecule-like absorption for thiolate-protected clusters.[47,61] It is worthy of note that a similar insulating-to-metallic transition of $Au_{55}(PPh_3)_{12}Cl_6$ clusters has been reported as induced by removal of the ligand shell of chlorine atoms through X-ray exposure.[62] All these results lead us to conclude that the icosahedral $Au_{13}(PPh_3)_4(SC_{12}H_{25})_4$ cluster is transformed to the cuboctahedral configuration once the protecting thiolate ligands are depleted from the cluster surface by a simple hexane treatment, although the precise 3D atomic structure of the cuboctahedral cluster remains to be determined due to the difficulty in crystallization of homogeneous clusters for X-ray crystallography measurements.[13−16]

Two-Step Process of the Hexane-Induced Structural Transformation. Summarizing the above results, we have demonstrated that a dramatic icosahedral-to-cuboctahedral structure transformation of $Au_{13}(PPh_3)_4(SC_{12}H_{25})_4$ nanoclusters could be driven by a simple solvent exchange of hexane for ethanol that selectively removes thiolate ligands from the cluster surface. The in situ UV−vis absorption and XANES measurements reveal that this transformation could be divided into two steps as illustrated in Figure 4 schematically. First, upon extracting the Au clusters from ethanol to hexane, the thiolate ligands are quickly depleted from the surface within 5 min (Figure 2). Due to the interplay between the "metallic"

dx.doi.org/10.1021/ja306923a | J. Am. Chem. Soc. 2012, 134, 17997−18003

behavior of the Au cores and the "molecular" behavior of the bonding environments,[30] the depletion of thiolates leads to a significant change in the character of the electronic structure, from semiconducting to metal-like. Second, without the protecting thiolate layers, the icosahedral structure of the phosphine-capped Au cores becomes unstable and degenerates into an *fcc* structure. This is a process to seek the minimization of the free energy, associated with some distortions of the surface and interior structures of the clusters relative to ideal *fcc* packing.[19,57] Compared with depletion of the thiolate ligands in the first stage, the structural rearrangement processes are much slower.

Finally, we discuss the variation of structural disorder of clusters before and after the structural transformation. An obvious reduction of the disorder degree σ^2 of the Au−Au bond (from 0.0102 to 0.0082 Å^2) is associated with the structural transformation. Generally, both ligands and solvent produce disorders in the nanoparticles that they surround, with the ligands having much greater effect.[63] When the Au clusters are protected by thiolates, the strong interactions between the Au core and the thiolates distort the cluster significantly, resulting in the I_h-like symmetry. After removal of thiolates, the weak interactions between the clusters and phosphine decrease the structural disorder and permit the clusters to adopt a more ordered structure with *fcc*-like atomic packing.

CONCLUSIONS

We report a structural transformation of Au_{13} nanoclusters from icosahedral to highly ordered cuboctahedral *fcc* atomic packing, driven by a facile solvent-exchange method. EXAFS and XANES analyses reveal that this transition arises from the hexane-induced selective removal of the thiolate ligands from the Au nanocluster surface. As a result of the dramatically alternated atomic structure, a great change in electronic structure is triggered as demonstrated by UV−vis absorption spectra that display a change from multiple absorption bands to a featureless absorption curve. In situ XANES and UV−vis absorption spectroscopy measurements further suggest a two-step process of the hexane-induced structural transformation: a quick thiolate desorption step followed by a relatively much slower geometric-structural rearrangement process. This work opens up the possibility of tailoring the structures and properties of metal nanoclusters by changing chemical environments. It also affords valuable clues to a long-unresolved fundamental scientific problem in nanoscience, i.e., the structural transformations during the evolution of clusters to nanocrystals.

ASSOCIATED CONTENT

Supporting Information

Fitting detail for FT EXAFS. This material is available free of charge via the Internet at http://pubs.acs.org.

AUTHOR INFORMATION

Corresponding Author

zhsun@ustc.edu.cn; yxie@ustc.edu.cn; sqwei@ustc.edu.cn

Notes

The authors declare no competing financial interest.

ACKNOWLEDGMENTS

This work is supported by the National Natural Science Foundation of China (Grant Nos. 11175184, 11135008, 10979044, 11079032, 11079004, and 10905058) and National Basic Research Program of China (2009CB939901). We thank NSRL and BSRF for the valuable beamtime. We are grateful to Prof. Manzhou Zhu, Mr. Shuxin Wang at Anhui University, and Dr. Songsong Bao at Najing University for their great help on MALDI-MS measurements.

REFERENCES

(1) Hakkinen, H. *Chem. Soc. Rev.* **2008**, *37*, 1847.
(2) Gao, Y.; Shao, N.; Pei, Y.; Chen, Z.; Zeng, X. C. *ACS Nano* **2011**, *5*, 7818.
(3) Zhu, Y.; Qian, H.; Zhu, M.; Jin, R. *Adv. Mater.* **2010**, *22*, 1915.
(4) Negishi, Y.; Tsunoyama, H.; Suzuki, M.; Kawamura, N.; Matsushita, M. M.; Maruyama, K.; Sugawara, T.; Yokoyama, T.; Tsukuda, T. *J. Am. Chem. Soc.* **2006**, *128*, 12034.
(5) Qian, H.; Zhu, Y.; Jin, R. *ACS Nano* **2009**, *3*, 3795.
(6) Lee, D.; Donkers, R. L.; Wang, G.; Harper, A. S.; Murray, R. W. *J. Am. Chem. Soc.* **2004**, *126*, 6193.
(7) Jin, R. *Nanoscale* **2010**, *2*, 343.
(8) Brust, M.; Walker, M.; Bethell, D.; Schiffrin, D. J.; Whyman, R. *J. Chem. Soc., Chem. Commun.* **1994**, 801.
(9) Negishi, Y.; Takasugi, Y.; Sato, S.; Yao, H.; Kimura, K.; Tsukuda, T. *J. Am. Chem. Soc.* **2004**, *126*, 6518.
(10) Chaki, N. K.; Negishi, Y.; Tsunoyama, H.; Shichibu, Y.; Tsukuda, T. *J. Am. Chem. Soc.* **2008**, *130*, 8608.
(11) Knoppe, S.; Boudon, J.; Dolamic, I.; Dass, A.; Bürgi, T. *Anal. Chem.* **2011**, *83*, 5056.
(12) Nimmala, P. R.; Dass, A. *J. Am. Chem. Soc.* **2011**, *133*, 9175.
(13) Jadzinsky, P. D.; Calero, G.; Ackerson, C. J.; Bushnell, D. A.; Kornberg, R. D. *Science* **2007**, *318*, 430.
(14) Heaven, M. W.; Dass, A.; White, P. S.; Holt, K. M.; Murray, R. W. *J. Am. Chem. Soc.* **2008**, *130*, 3754.
(15) Zhu, M.; Aikens, C. M.; Hollander, F. J.; Schatz, G. C.; Jin, R. *J. Am. Chem. Soc.* **2008**, *130*, 5883.
(16) Qian, H.; Eckenhoff, W. T.; Zhu, Y.; Pintauer, T.; Jin, R. *J. Am. Chem. Soc.* **2010**, *132*, 8280.
(17) Garzon, I. L.; Rovira, C.; Michaelian, K.; Beltran, M. R.; Ordejon, P.; Junquera, J.; Sanchez-Portal, D.; Artacho, E.; Soler, J. M. *Phys. Rev. Lett.* **2000**, *85*, 5250.
(18) Garzón, I. L.; Reyes-Nava, J. A.; Rodríguez-Hernández, J. I.; Sigal, I.; Beltrán, M. R.; Michaelian, K. *Phys. Rev. B* **2002**, *66*, 073403.
(19) Jiang, D.-e.; Tiago, M. L.; Luo, W.; Dai, S. *J. Am. Chem. Soc.* **2008**, *130*, 2777.
(20) Pei, Y.; Gao, Y.; Zeng, X. C. *J. Am. Chem. Soc.* **2008**, *130*, 7830.
(21) Häkkinen, H.; Walter, M.; Grönbeck, H. *J. Phys. Chem. B* **2006**, *110*, 9927.
(22) Cleveland, C. L.; Landman, U.; Schaaff, T. G.; Shafigullin, M. N.; Stephens, P. W.; Whetten, R. L. *Phys. Rev. Lett.* **1997**, *79*, 1873.
(23) Häkkinen, H.; Barnett, R. N.; Landman, U. *Phys. Rev. Lett.* **1999**, *82*, 3264.
(24) Häkkinen, H.; Moseler, M.; Landman, U. *Phys. Rev. Lett.* **2002**, *89*, 033401.
(25) Huang, W.; Bulusu, S.; Pal, R.; Zeng, X. C.; Wang, L. S. *ACS Nano* **2009**, *3*, 1225.
(26) Alexandridis, P. *Chem. Eng. Technol.* **2011**, *34*, 15.
(27) Donkers, R. L.; Lee, D.; Murray, R. W. *Langmuir* **2008**, *24*, 5976.
(28) Toikkanen, O.; Carlsson, S.; Dass, A.; Ronnholm, G.; Kalkkinen, N.; Quinn, B. M. *J. Phys. Chem. Lett.* **2010**, *1*, 32.
(29) MacDonald, M. A.; Zhang, P.; Chen, N.; Qian, H.; Jin, R. *J. Phys. Chem. C* **2011**, *115*, 65.
(30) MacDonald, M. A.; Chevrier, D. M.; Zhang, P.; Qian, H.; Jin, R. *J. Phys. Chem. C* **2011**, *115*, 15282.
(31) Newton, M. A. *Chem. Soc. Rev.* **2008**, *37*, 2644.
(32) Grubbs, R. B. *Nat. Mater.* **2007**, *6*, 553.
(33) Nie, Z.; Fava, D.; Kumacheva, E.; Zou, S.; Walker, G. C.; Rubinstein, M. *Nat. Mater.* **2007**, *6*, 609.

(34) Zhang, H. Z.; Gilbert, B.; Huang, F.; Banfield, J. F. *Nature* **2003**, *424*, 1025.
(35) Robinson, I. *Nat. Mater.* **2008**, *7*, 275.
(36) Li, Y. Y.; Liu, S. J.; Yao, T.; Sun, Z. H.; Jiang, Z.; Huang, Y. Y.; Cheng, H.; Huang, Y. Y.; Jiang, Y.; Xie, Z.; Pan, G. Q.; Yan, W. S.; Wei, S. Q. *Dalton Trans.* **2012**, *41*, 11725.
(37) Shichibu, Y.; Negishi, Y.; Tsukuda, T.; Teranishi, T. *J. Am. Chem. Soc.* **2005**, *127*, 13464.
(38) Qian, H. F.; Zhu, Y.; Jin, R. C. *Proc. Natl. Acad. Sci. U.S.A.* **2012**, *109*, 696.
(39) Zhang, H. J.; Schmid, G.; Hartmann, U. *Nano Lett.* **2003**, *3*, 305.
(40) Underwood, S.; Mulvaney, P. *Langmuir* **1994**, *10*, 3427.
(41) Creighton, J. A.; Eadon, D. G. *J. Chem. Soc., Faraday Trans.* **1991**, *87*, 3881.
(42) Aikens, C. M. *J. Phys. Chem. A* **2009**, *113*, 10811.
(43) Yao, T.; Sun, Z. H.; Li, Y. Y.; Pan, Z. Y.; Wei, H.; Xie, Y.; Nomura, M.; Niwa, Y.; Yan, W. S.; Wu, Z. Y.; Jiang, Y.; Liu, Q. H.; Wei, S. Q. *J. Am. Chem. Soc.* **2010**, *132*, 7696.
(44) Sun, Z. H.; Oyanagi, H.; Uehara, M.; Nakamura, H.; Yamashita, K.; Fukano, A.; Maeda, H. *J. Phys. Chem. C* **2009**, *113*, 18608.
(45) Jiang, D.-e.; Luo, W.; Tiago, M. L.; Dai, S. *J. Phys. Chem. C* **2008**, *112*, 13905.
(46) Yang, Y. Y.; Chen, S. W. *Nano Lett.* **2003**, *3*, 75.
(47) Zhang, P.; Sham, T. K. *Phys. Rev. Lett.* **2003**, 90.
(48) Marcus, M. A.; Andrews, M. P.; Zegenhagen, J.; Bommannavar, A. S.; Montano, P. *Phys. Rev. B* **1990**, *42*, 3312.
(49) Walter, M.; Akola, J.; Lopez-Acevedo, O.; Jadzinsky, P. D.; Calero, G.; Ackerson, C. J.; Whetten, R. L.; Gronbeck, H.; Hakkinen, H. *Proc. Natl. Acad. Sci. U.S.A.* **2008**, *105*, 9157.
(50) Menard, L. D.; Gao, S.-P.; Xu, H.; Twesten, R. D.; Harper, A. S.; Song, Y.; Wang, G.; Douglas, A. D.; Yang, J. C.; Frenkel, A. I.; Nuzzo, R. G.; Murray, R. W. *J. Phys. Chem. B* **2006**, *110*, 12874.
(51) Qian, H.; Zhu, M.; Lanni, E.; Zhu, Y.; Bier, M. E.; Jin, R. *J. Phys. Chem. C* **2009**, *113*, 17599.
(52) Shichibu, Y.; Negishi, Y.; Watanabe, T.; Chaki, N. K.; Kawaguchi, H.; Tsukuda, T. *J. Phys. Chem. C* **2007**, *111*, 7845.
(53) Menard, L. D.; Xu, H.; Gao, S.-P.; Twesten, R. D.; Harper, A. S.; Song, Y.; Wang, G.; Douglas, A. D.; Yang, J. C.; Frenkel, A. I.; Murray, R. W.; Nuzzo, R. G. *J. Phys. Chem. B* **2006**, *110*, 14564.
(54) Guliamov, O.; Frenkel, A. I.; Menard, L. D.; Nuzzo, R. G.; Kronik, L. *J. Am. Chem. Soc.* **2007**, *129*, 10978.
(55) Menard, L. D.; Xu, H. P.; Gao, S. P.; Twesten, R. D.; Harper, A. S.; Song, Y.; Wang, G. L.; Douglas, A. D.; Yang, J. C.; Frenkel, A. I.; Murray, R. W.; Nuzzo, R. G. *J. Phys. Chem. B* **2006**, *110*, 14564.
(56) Pundlik, S. S.; Kalyanaraman, K.; Waghmare, U. V. *J. Phys. Chem. C* **2011**, *115*, 3809.
(57) Tian, D.; Zhao, J. *J. Phys. Chem. A* **2008**, *112*, 3141.
(58) Haberlen, O. D.; Chung, S. C.; Stener, M.; Rosch, N. *J. Chem. Phys.* **1997**, *106*, 5189.
(59) Aikens, C. M. *J. Phys. Chem. C* **2008**, *112*, 19797.
(60) Hakkinen, H. *Nature Chem* **2012**, *4*, 443.
(61) Hussain, I.; Graham, S.; Wang, Z. X.; Tan, B.; Sherrington, D. C.; Rannard, S. P.; Cooper, A. I.; Brust, M. *J. Am. Chem. Soc.* **2005**, *127*, 16398.
(62) Boyen, H. G.; Kastle, G.; Weigl, F.; Ziemann, P.; Schmid, G.; Garnier, M. G.; Oelhafen, P. *Phys. Rev. Lett.* **2001**, *87*, 276401.
(63) Lal, M.; Plummer, M.; Smith, W. *J. Phys. Chem. B* **2006**, *110*, 20879.